



HAL
open science

Study of interactions between close HVDC links inserted in an AC grid: A mixed nonlinear and modal analysis approach

Iulian Munteanu, Bogdan Marinescu, Florent Xavier

► To cite this version:

Iulian Munteanu, Bogdan Marinescu, Florent Xavier. Study of interactions between close HVDC links inserted in an AC grid: A mixed nonlinear and modal analysis approach. *International Transactions on Electrical Energy Systems*, 2019, 10.1002/2050-7038.12266 . hal-02510539

HAL Id: hal-02510539

<https://hal.science/hal-02510539>

Submitted on 17 Mar 2020

HAL is a multi-disciplinary open access archive for the deposit and dissemination of scientific research documents, whether they are published or not. The documents may come from teaching and research institutions in France or abroad, or from public or private research centers.

L'archive ouverte pluridisciplinaire **HAL**, est destinée au dépôt et à la diffusion de documents scientifiques de niveau recherche, publiés ou non, émanant des établissements d'enseignement et de recherche français ou étrangers, des laboratoires publics ou privés.

Study of interactions between close HVDC links inserted in an AC grid: A mixed nonlinear and modal analysis approach

Iulian Munteanu¹, Bogdan Marinescu^{1,2}, Florent Xavier³

¹ Ecole Centrale Nantes-LS2N, 1 rue de la Noë, 44321 Nantes, France

³ Réseau de Transport d'Électricité, France

² corresponding author: bogdan.marinescu@ec-nantes.fr

January 3, 2019

Abstract

This paper focuses on interaction between two closed-connected high-voltage DC (HVDC) lines. This interaction is studied by employing high-fidelity nonlinear modeling in MATLAB[®]/Simulink[®] software environment. In order to describe the mechanism behind the HVDCs interaction, both nonlinear time-domain simulations and modal analysis of the coupled HVDC links, have been performed. System small-signal stability has been assessed and the path of interactions has been identified by computing the participations of various states in the oscillatory modes; this sets the preliminaries for a global, grid-oriented HVDCs control design approach. After the detailed analysis of newly-identified coupling oscillations, the minimal modeling requirements to put them into evidence have also been studied; this significantly facilitates the analysis in a realistic large-scale grid context.

Keywords: HVDC interactions, oscillatory modes, minimal modeling requirements, small-signal stability

1 Introduction. Scope of the paper

High-Voltage Direct Current (HVDC) lines are more and more used to reinforce transmission capacity of AC grids – [1]. As they are active elements, with multiple control degrees of freedom, their operation are likely to interfere due to geographic proximity (see, for example, the North-South HVDC projects in Germany or the ones on the border France-Spain - [2]), with potentially negative effects on their stability and the one of the neighbor AC zone.

HVDC lines interaction is an important issue for the power systems community – this is advocated by early publications that concerns HVDCs based upon

line-commutated converters (see, for example, [3]) and stated by international working groups ([4], [5]).

A thorough analysis of interactions between the converters of closed-connected HVDCs immersed in the AC grid is required, in order to properly qualify their closed-loop operating performance. In this sense, parallel voltage-source converters (VSC) operation in AC grid context have been studied in papers like [6], [7], where overall system stability is assessed by using converters input-admittance modeling. In [8] analysis of multi-terminal HVDC systems is approached, with focus on the DC system. Interaction modes between different VSCs has been revealed and their mechanism has been assessed. A particular and important situation occurs when the HVDC is inserted in a meshed AC system. In this case, not only interactions between the converters via the DC connections should be taken into account, but also direct connection via the AC grid. This results in dynamic coupling of the voltage/reactive power of the two converters AC connection points. In [9], control solutions are proposed in this context to reduce interaction between two close HVDCs using simplified phasor models.

These works revealed that entire HVDC line modeling at a certain level of detail is required, in order to properly identify and assess the phenomena that lie behind the HVDCs interactions.

The present work first approaches these interactions analysis by using electromagnetic transients (EMT)-based modeling which captures the VSC dynamic behavior for the full frequency range. Their nature and mechanism are explained *via* both nonlinear (in simulation) and modal analysis, run in a complementary way. Next, it is studied which are the minimal modeling requirements needed to emphasize the coupling phenomena. A preliminary study of these phenomena has been done in [10].

The approached system structure consists of two two-level HVDCs interconnected by means of a common AC power line, further denoted as ConAC – see Fig. 1. This is derived from the benchmark in [4], all AC lines and generators being simplified to impedances and infinite buses. The simplification allows to better identify dynamic properties belonging exclusively to HVDCs coupling. Also, this model is simple enough to be analytically treated in detail; by varying its parameters - especially the lengths of the AC lines and the level of injected power - one can take into account a wide range of realistic coupling situations. Thus, this benchmark is meaningful for studying the AC-DC interactions in the case of HVDC inserted in AC grids.

System behavior is assessed by means of modal analysis for continuous-time linear systems – [11], which offers a tool of determining of all (oscillatory) modes and of the degree of participation of system states in a certain mode. Originally used for stability issues in classical power system analysis, this approach may be applied to other types of complex systems, in which decoupling methods cannot be employed. A similar approach using multimodular converter (MMC)-based HVDC has been briefly presented in [12]. The present work extends system evaluation by thoroughly assessing states influence in shaping HVDC's interaction for various operating scenarios and parameters of the system. It is

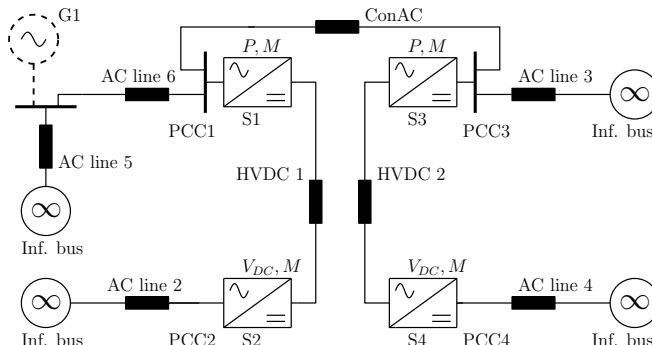


Figure 1: General overview concerning the interconnection of two HVDC lines by means of an AC line. Synchronous generator may be present into the AC grid, *AC line 1* is an equivalent of a series connection of *AC line 5* and *AC line 6*, in the case where G1 does not exist.

shown that this kind of interaction is of structural type, similar – to some extent – to the well known inter-area modes which exist between rotating generators. These interactions have been captured by means of a model able to replicate with sufficient accuracy transient phenomena within 0.1 Hz – 3 kHz frequency range (low-frequency oscillations, [13]).

The modeling approach in this paper has a twofold goal. It sets the preliminaries for a global, grid-oriented HVDCs control design approach and strives to precisely identify the circuit elements whose detailed modeling is relevant to replicate the HVDC-related phenomena in the frequency range of interest. This significantly facilitates the analysis in a realistic large-scale grid context.

Further, the paper is organized as follows. Section 2 goes on with system modeling aspects, while Section 3 presents the overall analysis approach. Sections 4 and 5 present results concerning the HVDCs interaction analysis. Section 6 identifies the minimal modeling required in order to capture the HVDC interactions. Section 7 reiterates the HVDC interaction analyses when the AC grid contains controlled synchronous generators. Section 8 concludes the paper.

2 Modeling approach

The approached system from Fig. 1 will be modeled by using the following general assumptions. AC environment is symmetrical and balanced and is modeled by AC infinite buses and series reactances. AC-DC converters are lossless and are switching instantaneously, the converters switching dynamics being neglected. The connection transformer, usually placed at a certain Point of Common Coupling (PCC), has negligible magnetizing impedance and presents no magnetic saturation phenomena; for sake of analysis, its dynamic behavior and the one of the phase reactor will be lumped into a single RL passive element, the

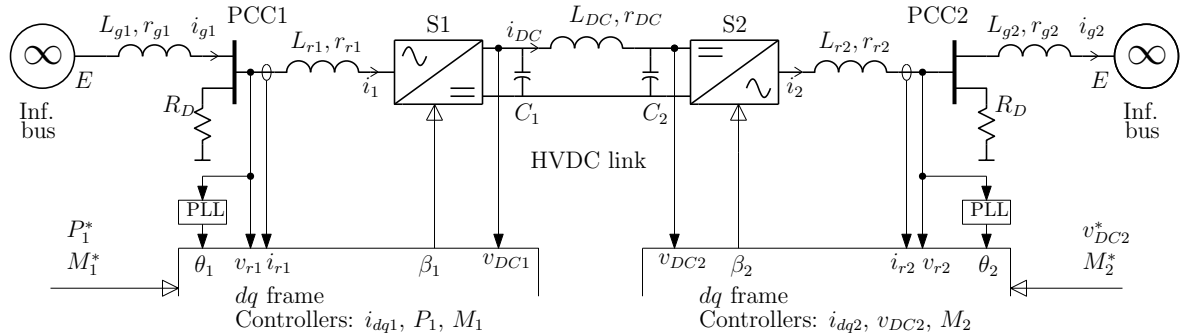


Figure 2: Simplified diagram of HVDC transmission line and its overall control.

whole AC system becomes rated at a common voltage value like in [10] – this is also suggested in Fig. 2. The interconnection AC line (ConAC in Fig. 1) is modeled as an RL circuit element. Concerning the synchronous generator, the modeling assumptions consider sinusoidal evolutions of voltages and currents in the stator, no magnetic saturation and neglect effects of rotor amortisseurs (only the field circuit is considered in the rotor).

2.1 HVDC structure and assumptions

One considers a symmetrical monopole VSC-HVDC transmission power link whose equivalent diagram (with lumped DC lines and equivalent capacitors) is depicted in Fig. 2. It has two converter stations that employ bidirectional 3-phase AC-DC power converters, interlinked by means of DC cables and connected to equivalent AC grids, represented by infinite buses. Subscript indexes of various variables designate the station to which these variables belong.

VSC switched operation takes place at a high frequency with respect to the main dynamics and requires filtering elements on each station: capacitors on DC side and line reactors on AC side.

VSCs of HVDC link are operated in pulse-width modulation (PWM) in order to interchange averaged sinusoidal variables with AC grid. The converter switching dynamics are neglected and VSCs are modeled here by their averaged model, obtained by replacing converter switching functions with their sliding averages – see [14].

2.2 HVDC dq frame modeling

The power subsystem model results from analyzing the electrical interactions between VSC and infinite bus through passive circuit elements. The model is then described in **rotating dq frame linked to the infinite bus**; on d channel one conveys active power and on q channel reactive power. One writes

dynamic model of HVDC station S1 connected to the equivalent grid, by means of equation set (1):

$$\begin{cases} L_{r1}\dot{i}_{rd1} &= \omega L_{r1} \cdot i_{rq1} - 0.5v_{DC1} \cdot \beta_{rd1} + v_{rd1} - r_{r1} \cdot i_{rd1} \\ L_{r1}\dot{i}_{rq1} &= -\omega L_{r1} \cdot i_{rd1} - 0.5v_{DC1} \cdot \beta_{rq1} + v_{rq1} - r_{r1} \cdot i_{rq1} \\ C\dot{v}_{DC1} &= 1.5(i_{rd1} \cdot \beta_{rd1} + i_{rq1} \cdot \beta_{rq1}) - 2i_{dc} \\ L_{g1}\dot{i}_{gd1} &= \omega L_{g1} \cdot i_{gq1} - v_{rd1} + E - r_{g1} \cdot i_{gd1} \\ L_{g1}\dot{i}_{gq1} &= -\omega L_{g1} \cdot i_{gd1} - v_{rq1} - r_{g1} \cdot i_{gq1} \\ v_{rd1} &= (i_{gd1} - i_{rd1}) \cdot R_D \\ v_{rq1} &= (i_{gq1} - i_{rq1}) \cdot R_D, \end{cases}, \quad (1)$$

where i_{rd1} and i_{rq1} are the reactor current components, i_{gd1} and i_{gq1} are the AC line current components, v_{rd1} and v_{rq1} are the PCC voltage components, E is the infinite bus voltage amplitude, ω is the AC system frequency and v_{DC1} is the DC line voltage at the concerned VSC (capacitor filter voltage). L_{r1} and r_{r1} are the reactor inductance and resistance, respectively, L_{g1} and r_{g1} are the AC line inductance and resistance, respectively and C_1 is the value of DC-side capacitor. β_{rd1} and β_{rq1} are plant (station S1) control inputs. The first three equations from set (1) actually represent VSC model as is classically described in the concerned bibliography – *e.g.*, [15, 16]. The first two equations model interactions of two AC voltage sources connected by means of an RL passive element, and the third equation represents voltage balance on the DC filter capacitor. Note that d and q channels are cross-coupled. Voltage v_{rd1} is obtained by balancing currents i_{rd1} and i_{gd1} on a local very large resistive load (R_D), situated at PCC, same remark being applicable to channel q .

Equations (1) may be completed with the DC line dynamic, given by equation (2). Here, L_{DC} and r_{DC} are the inductance and the resistance of the high-voltage DC line, respectively and v_{DC2} is DC voltage at station S2, see HVDC link layout in Fig. 2.

$$2L_{DC}\dot{i}_{DC} = v_{DC1} - v_{DC2} - 2r_{DC} \cdot i_{DC}. \quad (2)$$

Further, concerning the station control, its overall scope is to track imposed levels of both active and reactive power values, on d and q channels, respectively. In the present work, VSC classical control structure has been adopted, VSC controllers being developed in a new dq frame linked to the PCC1 by means of a phase locked loop (PLL), like in [15]. This basically requires a changing of dq coordinates from the infinite bus to a frame linked to PCC1; therefore, the estimation of the PCC1 angle is done by using a PLL which phase detector is the so-called Kron transform – see [17, 10]. The new variables expressed in the **new (PCC-linked) dq frame** will be denoted by i_{dq1} , β_{dq1} and v_{dq1} (for station S1). Relation with variables from equation (1) is given by the Kron transform – see equations (3) for the case of currents and duty ratios:

$$\begin{cases} i_{d1} &= i_{rd1} \cdot \cos \delta_1 - i_{rq1} \cdot \sin \delta_1 \\ i_{q1} &= i_{rd1} \cdot \sin \delta_1 + i_{rq1} \cdot \cos \delta_1 \\ \beta_{rd} &= \beta_d \cdot \cos(-\delta_1) - \beta_q \cdot \sin(-\delta_1) \\ \beta_{rq} &= \beta_d \cdot \sin(-\delta_1) + \beta_q \cdot \cos(-\delta_1) \end{cases}, \quad (3)$$

with δ_1 being the phase shift between the two frames.

Using measurements from the station S1 (PCC1) (currents and voltages from d and q axis in PLL frame) one may compute active and reactive power, respectively as:

$$\begin{cases} P_1 &= 1.5 (v_{d1} \cdot i_{d1} + v_{q1} \cdot i_{q1}) \\ Q_1 &= 1.5 (v_{d1} \cdot i_{q1} - v_{q1} \cdot i_{d1}). \end{cases} \quad (4)$$

The classic control structure employs inner current control loops with cross-decoupling $d-q$ structure that use proportional-integral laws – see, for example, [16]. Current components references are provided by the outer control loops.

On q channel, the outer loop aims at tracking a composite variable representing a mix between the PCC1 voltage amplitude, v_{PCC} and reactive power, Q_1 . This variable, introduced in [18], is denoted in the sequel by M_1 , and is given by equation (5):

$$M_1 = v_{PCC1} + \lambda \cdot Q_1, \quad (5)$$

λ being the reactive power coefficient (measured in kV/kVar) and PCC voltage amplitude is $v_{PCC1} = \sqrt{v_{d1}^2 + v_{q1}^2}$.

It can be shown that the plant to be controlled can be expressed as a gain, therefore a simple integral controller can be used for PCC voltage amplitude and for reactive power, as in [16].

On d channel, either active power at PCC or DC-link voltage can be controlled within the corresponding outer loop. VSC of station S1 is controlled in active power, HVDC link DC voltage being ensured by station S2. In this case the plant can be easily approximated with a gain, which is PCC voltage amplitude – see first equation of set (4), by considering $v_{q1} \approx 0$. In this case also one usually employs an integral controller.

The overall control law is expressed in dq frame linked to PCC and is given by equations set (6) – see [16]:

$$\begin{cases} \beta_{d1} &= -K_{pc} (1 + 1T_{ic}s) (i_{d1}^* T_{ic}s + 1 - i_{d1}) + 2\omega L_{r1} v_{DC1} \cdot i_{q1} \\ \beta_{q1} &= -K_{pc} (1 + 1T_{ic}s) (i_{q1}^* T_{ic}s + 1 - i_{q1}) - 2\omega L_{r1} v_{DC1} \cdot i_{d1} \\ i_{d1}^* &= 1T_{iPS} \cdot (P_1^* - P_1) \\ i_{q1}^* &= 1T_{iMS} \cdot (M_1^* - M_1), \end{cases} \quad (6)$$

where s is the Laplace operator and variables $\langle \cdot \rangle^*$ denote the associated set-points. K_{pc} and T_{ic} are the proportional gain and integrator constant of PI current controllers, T_{iP} is the active power controller integrator constant and T_{iM} is the reactive power controller integrator constant. β_{d1} and β_{q1} are components of converter duty ratio, β_1 , in (PCC1-linked) dq frame.

Note that, in real-world application, a generic PCC phase angle is extracted from its voltages by using a three-phased PLL system and all computations in the station control system are done in the coordinates linked to the PLL angle. It is known that the PLL synchronizes on PCC angle with a certain dynamic (depending on its internal controller parameters), its actual value being delayed from the PCC angle in dynamic regime. Thus, it induces a non negligible effect on the overall dynamic behavior of the controlled VSC, negatively impacting its stability – see [19]. Here, the adopted PLL structure is the one represented in Fig. 3. One may show that, by using Kron transform as a phase detector, this structure outputs the same angle as a 1st order classical PLL and exhibits the same dynamics. In short, in steady state this loop outputs the necessary value of angle δ that nullifies the voltage v_{q1} ; this angle represents the phase shift between the PCC-linked and infinite bus-linked dq frames.

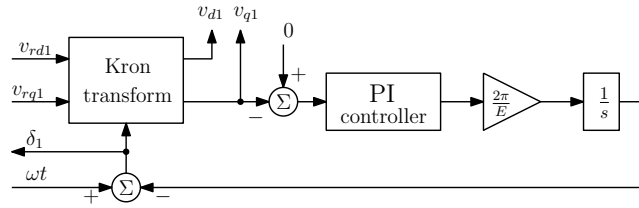


Figure 3: PLL structure using Kron transform as phase detector (station S1).

PLL dynamics intervene twice: in i_{d1} and i_{q1} computation in direct Kron transform (*i.e.*, in variables measurement) and in β_{rd1} and β_{rq1} computation (actuation in inverse Kron transform), by means of angle δ_1 with a non-negligible influence in the overall closed-loop dynamic behavior. Its modeling is the same for all four stations in the benchmark in Fig. 1.

Concerning station S2, the plant is modeled similarly as in the case of station S1, by using equations (1). The inner control loop is the same, but the outer loop is different: on q channel, its target is to track M_2^* variable, similarly as station S1; on d channel its target is different – to regulate the HVDC line voltage at the desired value.

Note that the third equation of set (6) is valid only for the power-controlled station/VSC, which is the case of station S1. Station S2, which uses voltage control, employs equation (7) instead – see [20].

$$i_{d2}^* = K_{pv} (1 + 1T_{iv}s) \cdot (v_{DC2}^* - v_{DC2}) \quad (7)$$

Therefore, in HVDC1 one imposes active power value to station S1 to be injected/draind from the grid; station S2 will drain/inject the required amount of active power necessary to balance the HVDC voltage. The control system of a single HVDC line has been tuned in order to obtain pertinent performances for i_d and i_q : damping at around 0.65 - 0.85 and time constant 5 ms for the inner loops, for typical scenarios and operating points. Time response for outer loops

corresponds to ≈ 17 ms for v_{DC} control loop and to 20 - 30 ms for active power P and variable M . All these outer loops have variable damping depending on grid equivalent short-circuit ratio (SCR) at the corresponding station, (*i.e.*, the AC impedance) and on the operating point. SCR value is classically defined as in [21]:

$$SCR = S_{AC}P_{DCr},$$

where S_{AC} is station bus (PCC) short-circuit capacity and P_{DCr} is HVDC rated power.

2.3 Benchmark modeling

Further, the second HVDC in Fig. 1 is modeled in the same manner as the HVDC in Fig. 2 and detailed in the section above. Similarly, station S3 is power-controlled and station S4 is voltage-controlled.

ConAC line is modeled as a RL branch, by using equations similar to equations (4) and (5) from equation set (1).

The synchronous machine model employed in this paper is the classical one, expressed in rotor-linked dq frame as given, e.g., in [22] (step-up connexion transformer being ideal). A classical control structure, containing two loops, one for terminal voltage control (excitation) and one for output power control (turbine-generator governor) has been employed [22]. The parameters from the control structure have been chosen following classic and best engineering practices, in order to match the following target dynamic performance (in terms of power): rise time of 25-30 s with a suitable damping (*e.g.*, larger than 0.2, for the operating range 10%-100% of rated power). It has been further tested on an equivalent grid including an infinite bus and AC line lengths between 50 and 400 km.

3 A mixed analysis approach

The setup in Fig. 1 has been implemented in Simulink[®] toolbox of the MATLAB[®] software by means of *nonlinear modeling* detailed in Section 2. On this model, extensive simulations have been performed in order to emphasize the behavior of the two coupled HVDC links and to make a preliminary assessment of their interaction.

In a second step, *system linearization and modal analysis* are targeted in order to better quantify the HVDCs interaction. As a preliminary step, all system states (integrators) in the Simulink[®] diagram are labeled with suitable identifiers (*e.g.*, "int PI iq3" means the state associated with the i_{q3} current controller integrator). Then, after eliminating nonessential nonlinearities (saturations, *etc*), linearization is done numerically, by using the *Linear analysis* tool available in the above-cited software around a steady-state operating point, corresponding to a certain scenario. For consistency, in all scenarios the input is chosen as M_1^* (the setpoint) and the output as M_1 , although any of variables P_k

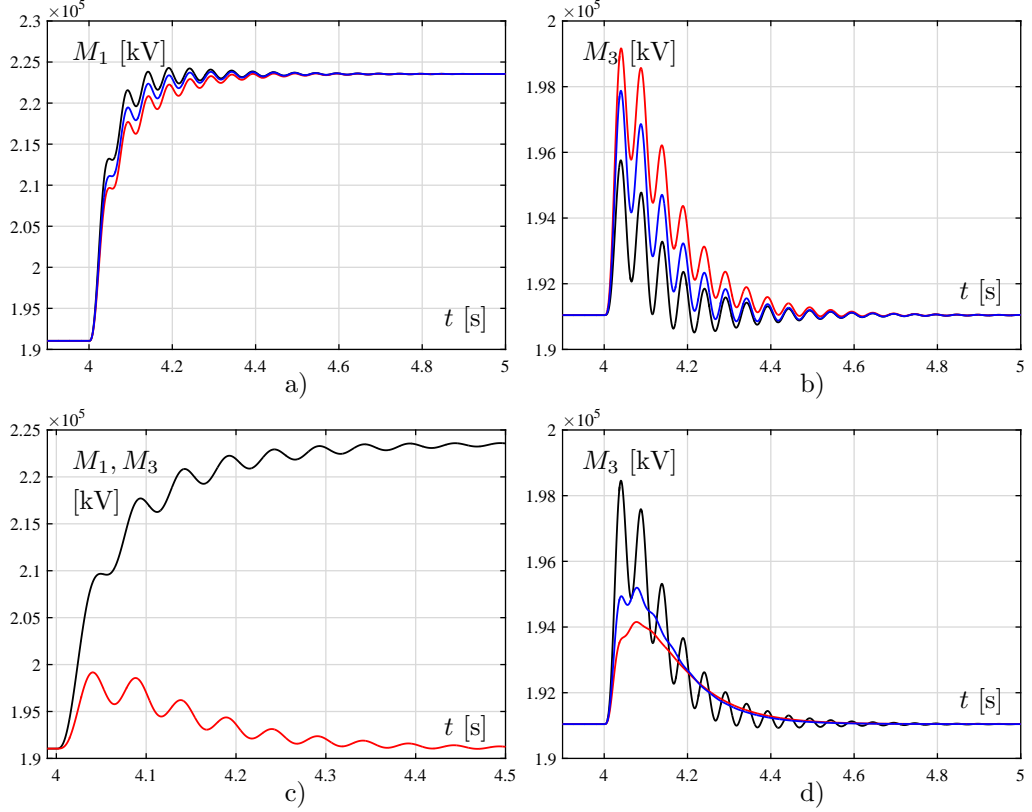


Figure 4: Nonlinear system response to a M_1^* step: a) and b): nonlinear system response at M_1 step point step variation, for various ConAC line lengths black – 500 km, blue – 200 km, red – 100 km; c): detail of M_1 (black) and M_3 (red) evolutions at a M_1 setpoint step, where ConAC length is $L_{AC} = 100$ km; d): M_3 evolution at M_1 step point step variation, for various SCR values (black – 3.5, blue – 5, red – 7.5).

and M_k with $k = 1..4$, may be set as output. The linearization outputs system state matrix, A , together with a vector of state variables labels.

Modal analysis for continuous-time linear time-invariant system starts with the state matrix. Based on this matrix, normalized right eigenvectors v_i and left eigenvectors w_i , which verify

$$\begin{cases} A \cdot v_i &= v_i \cdot \lambda_i \\ w_i \cdot A &= \lambda_i \cdot w_i \end{cases}, \quad (8)$$

with $w_i \cdot v_j = 0$ for $i \neq j$ and $w_i \cdot v_j = 1$ for $i = j$ – see [11] – are determined, where λ_i are the eigenvalues of A .

The participation factor of variable x_j in mode i is computed as the product between elements j of vectors w_i and v_i :

$$p_{ji} = (w_i)_j \cdot (v_i)_j, \quad (9)$$

see [11] for quick reference.

One determines participation factors for all state variables and for all system modes, *i.e.*, the so-called participation factor matrix (square matrix of system dimension) – see [11]. Absolute values of participation factors are further used, to compare the influence of variables that intervene in a certain mode. All oscillatory modes are analyzed in order to emphasize the systems’ shape of oscillations. The ones poorly-damped and related to electrical couplings (*i.e.*, which involve distant devices) are of particular interest.

Results concerning this analysis will be presented in the next sections by means of scenarios that can be split into two categories: with or without G1 generator connected in the AC grid. Irrespective of the situation, only parameters and setpoints of stations S1 and S3 will change; stations S2 and S4 setpoints are voltages $v_{DC2}^* = v_{DC4}^* = 640$ kV and $M_2^* = M_4^* = 332$ kV (rated values). Their associated SCR is always constant, at ≈ 5 . The values considered for ConAC line length correspond to the initially-stated “close” HVDC lines context. Setpoints of the synchronous generator are constant determining a steady state at around $P_e = -400$ MW, in terms of active power and at about $Q_e = -100$ MVAR, reactive power. Both high-voltage DC lines have a length of 200 km. In this paper passive sign (load) convention has been used.

4 Coupling mode identification by nonlinear simulation

4.1 Time-domain numerical simulations.

In order to make a preliminary assessment of the coupling behavior, one choses the structure **without generator G1**, in which the operating context consists in injecting into the AC grid active power values $P_1 = -500$ MW and $P_3 = -250$ MW and in maintaining $M_3 = 332$ kV (at rated value); also, both S1 and S3 have the same SCR=5 value. Simulations on the nonlinear Simulink[®] model have been performed and a large step of M_1 setpoint, has been imposed.

Fig. 4 a) presents M_1 variable evolutions (local control loop voltage tracks setpoint variation), and Fig. 4 b) M_3 evolutions – corresponding control loop rejects the perturbation, both for various lengths of interconnection line, ConAC. System’s dynamic behavior has two main components: a damped behavior whose frequency becomes smaller as ConAC line length decreases, and a second undamped behavior, whose frequency is around 20 Hz (see also Table 1) and which is an oscillating mode that couples the two HVDCs. Indeed, in Fig. 4 c) a detail of M_1 (black) and M_3 (red) evolutions at a M_1 setpoint step (ConAC is of 100 km) is shown. The same transient dynamics can be noted on both

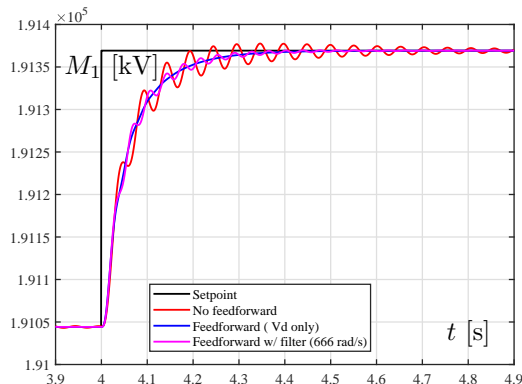


Figure 5: Nonlinear system response to a M_1^* step: black line – set-point evolution, red line – case without feedforward, blue line – case with feedforward, magenta line – case with filtered feedforward.

outputs – oscillations have the same frequency, the same damping and the same phase, suggesting that the two input-output transfer channels are coupled, as their oscillations are due to the same mode.

4.2 Why not using feedforward component in current loops?

An alternative common approach is to use a feedforward component in the low level control loops to obtain better behavior in terms of stability. This is indeed useful for the case of a weak grid, where PCC voltage varies significantly – *i.e.*, v_{d1} in 2nd equation of (1). The feedforward is done by measuring v_{d1} voltage and reinjecting it into the duty cycle control law, *i.e.*, in 2nd equation from (6).

For sake of comparison, this alternative solution has also been implemented in S1-S4 controls and Simulink[®] numerical nonlinear simulations have been performed.

One observes in Fig. 5 that the voltage response is totally smoothed – blue line in the case where ideal PCC voltages measuring would be available. This means that the oscillatory modes are not present anymore (or are sufficiently damped) and the feedforward action is effective. However, in real-world applications, the measure of PCC voltage is affected by filtering. When the feedforward component uses the filtered value of PCC voltage, the system response becomes oscillatory, again – see the magenta line in Fig. 5. So the new dynamics introduced by the filtered PCC voltages appear to counteract the effect of a genuine feed-forward and thus the increase in the system complexity is unjustified.

Further, the analysis will be done without the feedforward components in the low-level control loops – *i.e.*, as in Subsection 4.1, by using equations (6), for sake of being coherent with an analysis/design of the system in its totality, free of local and only partially effective control “patches”.

5 Modal analysis of HVDCs interaction

5.1 Parametric analysis for various operating scenarios

For the above-described context, the nonlinear system is linearized around the associated steady-state operating point, by using numerical tool in Simulink[®] software; thus, a 62-states linear model is obtained. Modal analysis algorithm – based upon equations (8) and (9) – is applied and the previously-observed oscillatory mode (see Fig. 4), which will be further referred to as *Mode 29*, is identified. Its frequency is around 20 Hz and it is poorly damped in some situations which will be discussed next. Most participative states in *Mode 29* are the ones contained into the inner control loops (PLL and current controllers), see also Table 2. Variables belonging to S1 – from the HVDC link 1 – and S3 – from the HVDC link 2 – have the most important contributions to *Mode 29*. This confirms the conclusions of the previous time-domain analysis, that the two HVDCs interact.

Next, variations of *Mode 29* parameters with respect to the operating context will be studied.

The first scenario involves modal analysis for three different SCR values at stations S1 and S3. Steady-state active power values are $P_1 = -500$ MW and $P_3 = -250$ MW, M variables $M_1 = M_3 = 332$ kV and ConAC line length is $L_{AC} = 150$ km.

Fig. 4 d) shows M_3 evolution (non-linear system simulations) at a step on M_1 setpoint. Note that the system is less damped as SCR values at both S1 and S3 are smaller (the grid is weaker). This can also be seen in the modal analysis results. Table 1 (left side) shows *Mode 29* main parameters for the three SCR values. Frequency has not an important variation, but the damping is severely decreasing with SCR, thus affecting the system stability.

Fig. 6 a), which contains the system pole's evolution as SCR decreases, shows the same trend. Further reduction of SCR values makes the system unstable. Table 2 contains ranking of most participative system states in *Mode 29* for two values of SCR. Note that most participative states belong to inner loop controllers and to PLLs of either station S1 and S3.

The second scenario concerns modal analysis for various active power values (positive/power draw or negative/power injection) required for stations S1 and S3. The set-up presumes a ConAC line of 150 km, both S1 and S3 maintain variables M_1 and M_3 at their rated values (*i.e.*, 332 kV); SCR is the same for S1 and S2, *i.e.*, 3.5. Stations S2 and S4 follow operation of stations S1 and S3 respectively, by regulating DC voltage at the rated value (640 kV).

Table 1 (right side) shows *Mode 29* parameters variation with P_1 and P_3 values. Damping of *Mode 29* is lowest when both S1 and S3 inject power in AC grid. This is also visible on Fig. 6 b), showing variation of pole associated with *Mode 29* with respect to power levels. Ranking of first nine states participating in *Mode 29* are shown in Table 3. The inner loop (current) controllers states, including PLLs (either the PLL integrator or its PI controller), have the most important participation in this mode. Note also, that these states belong to

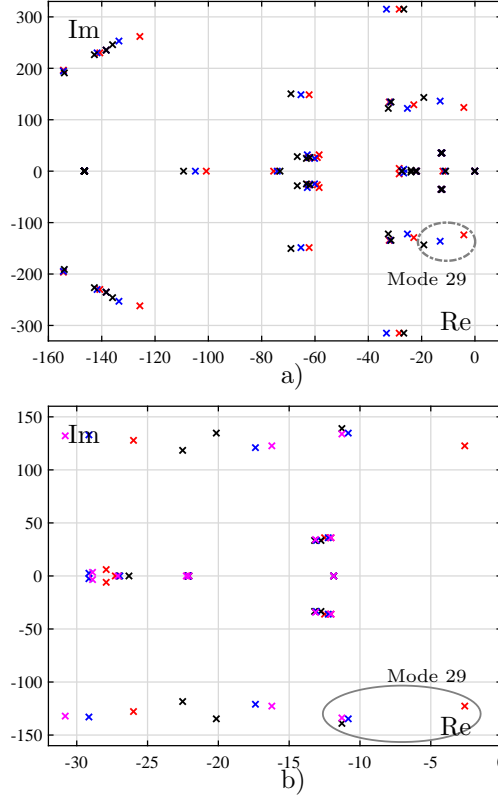


Figure 6: a) System pole-zero maps for various SCR values: black – 5, blue – 4, red – 3; b) System pole-zero maps for various P_1 and P_3 setpoints; red: $P_1 = -500$ MW, $P_3 = -600$ MW, blue: $P_1 = -500$ MW, $P_3 = +600$ MW, magenta: $P_1 = +500$ MW, $P_3 = -600$ MW, black $P_1 = +500$ MW, $P_3 = +600$ MW.

stations that inject active power. For example, ranking in column 3 of Table 3, corresponds to case where S1 draws power and S3 injects power from/in their AC grids. Therefore, S2 injects power and S4 draws power in/from their AC grids in order to maintain DC voltage at the prescribed value. States belonging to stations S2 and S3 are the most participative. Table 3 shows that this remark holds for all analyzed cases.

Notice that the coupling mode is systematically better damped in scenarios where power-controlled stations (S1 and S3) draw power – see the right side of Table 1. Also, note that in all cases the states belonging to the ConAC line do not significantly intervene in *Mode 29*. Also, states belonging to VSC reactors, AC lines and low-level loop prefilters – see equations (6) – may also be significantly involved in the participation mix.

5.2 Modal sensitivity analysis *wrt.* to ConAC line length

This subsection aims at quantifying the influence of the interconnection line length, L_{AC} on the interaction *Mode 29*, based on results presented in [24] and [25]. From the definition of sensitivity one can show that variation of eigenvalues λ_i of system matrix A , *wrt.* to parameter L_{AC} may be expressed as in equation (10):

$$S_{Li} = \partial\lambda_i \partial L_{AC} = \sum_{kj} \partial\lambda_i \partial a_{kl} \cdot \partial a_{kl} \partial L_{AC}, \quad (10)$$

for all $i = 1..n$, n being the system order and a_{kl} the element of line k and column l of matrix A .

A single term from equation (10), further called partial sensitivity s_{kl} , may be written as:

$$s_{kl} = \partial\lambda_i \partial a_{kl} \cdot \partial a_{kl} \partial L_{AC} = w_{ik} v_{il} \cdot \partial a_{kl} \partial L_{AC}, \quad (11)$$

with $k, l = 1..n$, v and w the right and left eigenvectors of λ , respectively. Therefore, the sum of all elements described by equation (11) represents the total sensitivity of a certain mode with respect to the parameter L_{AC} .

Further, equation (11) is used to estimate the elements of variable S_{L29} , *i.e.*, sensitivity of *Mode 29* *wrt.* to ConAC length; this is done by employing two system configurations, each of them having different ConAC line length. The procedure runs as detailed bellow.

- #1. First, one obtains linearized model (and hence matrix A_1 , eigenvectors v and w) for a ConAC length $L_{AC} = 100$ km. Then, the procedure is repeated for a longer line of $L_{AC} = 200$ km and one obtains matrix A_2 .
- #2. One easily computes elements $\frac{\Delta a_{kl}}{\Delta L_{AC}}$ (an estimate of the last component in equation 11), by subtracting matrix A_1 from A_2 , $\Delta A = A_2 - A_1$, and obtaining variables Δa_{kl} , for all $k, l = 1..n$.
- #3. Only the significant values $\frac{\Delta a_{kl}}{\Delta L_{AC}}$, implying an important dependence with the ConAC length, are further used (all other are discarded). One obtains a vector containing this variables by sweeping matrix ΔA line by line. One also gets a vector with line indices, k and another one with column indices, l corresponding to the preserved values.
- #4. The selected mode being $i = 29$, one can also select eigenvectors v_{29l} and w_{29k} , by sweeping vectors of column indices and of line indices obtained at step #3. Then, one computes partial sensitivities s_{kl} for all the significant values $\frac{\Delta a_{kl}}{\Delta L_{AC}}$, by using equation (11), and A_1 eigenvectors.
- #5. Summation of all partial sensitivities computed at step #4 gives the *Mode 29* sensitivity *wrt.* ConAC line length.

Further, one studies this sensitivity when the system has a symmetrical structure and when it has a certain asymmetry. Two asymmetrical cases have been analyzed. First, the asymmetry is given by different SCR values at stations S1 and S3. Secondly, the asymmetry is functional (due to power flow), active power values at S1 and S3 are different, *i.e.*, ConAC line is charged.

5.2.1 Scenario 1: symmetric structure

Both active power levels, P_1 and P_3 are -500 MW (injected into AC grid). First, one considers both infinite buses AC1 and AC3 with the same $SCR=3.5$. Fig. 7 a) shows the partial sensitivities, for this case. Note that only six values $\frac{\Delta a_{kl}}{\Delta L_{AC}}$ have been taken into account (the others are insignificant); j is the index in $\frac{\Delta a_{kl}}{\Delta L_{AC}}$ (or else in vectors k and l). The total sensitivity value is very small $S_{L29} \approx 3.4e - 6$, which suggests quasi invariance of *Mode 29* parameters (and associated participation factors) with ConAC line length.

5.2.2 Scenario 2: structural asymmetry

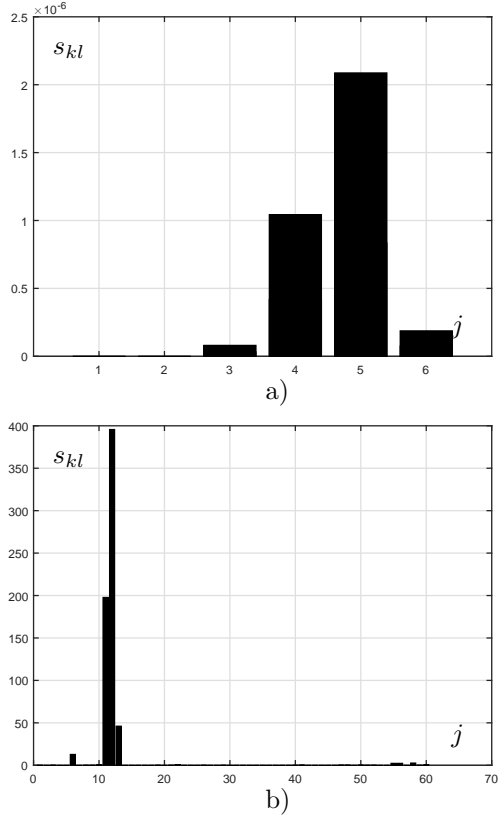


Figure 7: Partial sensitivities for: a) symmetric case (equal SCR s at AC1 and AC3); b) structural asymmetric case (AC3 has 10% smaller SCR than AC1).

In a second case, one considers a small difference between SCR values in infinite buses AC1 and AC3; the first one is 3.5, the latter being 10% smaller. Fig. 7 b) shows the magnitude of sensitivities for this second case. This case

has 62 significant values that have been retained. Note that in this second case partial sensitivities are significantly larger *wrt.* the first case; total sensitivity is $S_{L29} \approx 659.4$.

To conclude, as the system is symmetric (not only from the structure point of view, but also from the power flow point of view), the sensitivity of *Mode 29* *wrt.* ConAC line length is extremely small. However, even a small imbalance in system structure determines a significant sensitivity of the studied mode *wrt.* L_{AC} .

5.2.3 Scenario 3: asymmetry in power flow

This case considers symmetrical system structure *wrt.* middle point of ConAC line. This means that SCR values are equal for S1 (AC line 1) and S3 (AC line 3); this is also valid for S2 and S4. However, active power levels imposed to each of stations S1 and S3 differ. Table 4 shows the output of the above-detailed procedure for four different power flow situations. Likewise in the previous scenario, in the asymmetrical cases (when ConAC line is loaded) the total sensitivity of *Mode 29* *wrt.* ConAC length is significantly higher than in the symmetrical ones. Fig. 8 shows the distribution of partial sensitivities for the asymmetrical power flows. In this cases it is expected that parameters of this mode have important variations with the line length variation. This analysis also implies that, in the symmetric cases, *Mode 29* is insensitive to this parameter.

6 Minimal modeling to capture the HVDC links interactions

Analysis above was carried out with a very detailed modeling in order to be sure not to lose any relevant dynamics. The question is now to state which are the minimal modeling requirements to capture the coupling mode put into evidence between the two HVDCs. This is done to further facilitate large-scale AC grid studies. For this, separate influence of certain dynamics over the HVDCs interaction, are analyzed. Scenarios considered next have: ConAC of 150 km, SCR1=3.5 and SCR3 = 3 (which makes a slight structural unbalance between S1 and S3). Steady-state operating point is imposed by $P_1 = +500$ MW and $P_3 = -600$ MW in order to have operational asymmetry. Steps of reference voltage are applied at S1 (M_1^* is the input, M_1 is the system output).

6.1 System containing ConAC line without dynamics

As it has been recalled before, RL-based ConAC line model is given by equations four and five of set (1), in the form of equations (12):

$$\begin{cases} L_c \dot{i}_{cd} &= \omega L_c \cdot i_{cq} + v_{rd1} - v_{rd3} - r_c \cdot i_{cd} \\ L_c \dot{i}_{cq} &= -\omega L_c \cdot i_{cd} + v_{rq1} - v_{rq3} - r_c \cdot i_{cq} \end{cases}, \quad (12)$$

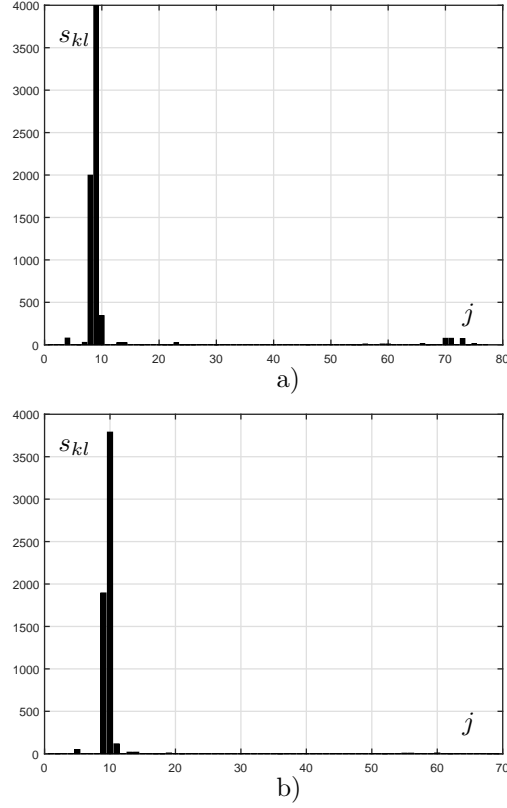


Figure 8: Partial sensitivities for: a) $P_1 = -500$ MW, $P_3 = +500$ MW; b) $P_1 = +500$ MW, $P_3 = -500$ MW.

where i_{cd} and i_{cq} are ConAC line current components, v_{dr1} and v_{qr1} are the PCC1 voltage components at station S1 and v_{dr3} and v_{qr3} the PCC3 voltage components at station S3. L_c and r_c are the inductance and the resistance of ConAC, respectively.

If one nullifies the derivatives on both d and q axis and neglects the line resistive effect, one obtains an algebraic model of the ConAC line, yielding its current components as:

$$\begin{cases} i_{dc} &= \frac{1}{\omega L_c} (v_{qr1} - v_{qr3}) \\ i_{qc} &= -\frac{1}{\omega L_c} (v_{dr1} - v_{dr3}). \end{cases} \quad (13)$$

Further, the benchmark in Fig. 1 is implemented by using ConAC model given by equations (13). As previously, one linearizes (by using numerical tool in Simulink[®]) system around the corresponding steady-state operating point and a 60th order system is obtained.

Fig. 9 a) shows the step response of the newly-obtained, reduced order system, in red *vs* the one of the full-order original system, described by the black trace. Note that the response is quite similar, the reduced-order system also has an undamped response of about the same frequency and damping. This observation is backed by the pole maps in Fig. 9 b). The concerned pole pair, situated at about 20 Hz, is perfectly superposed over the original system with full dynamics (see red and black crosses).

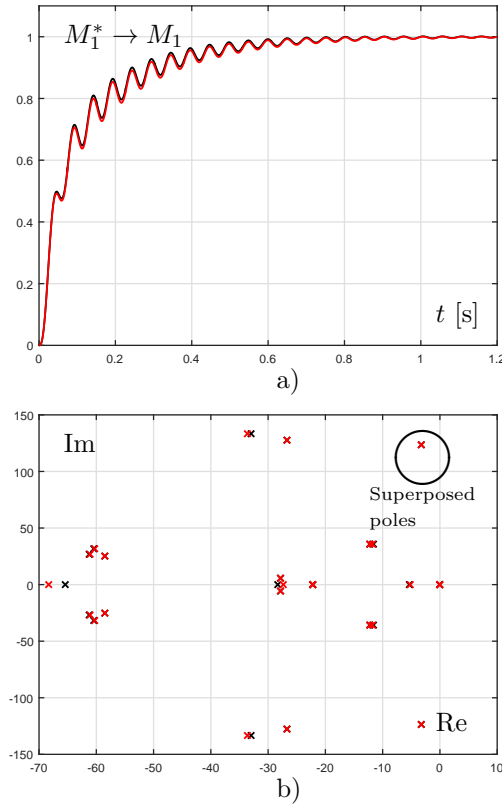


Figure 9: Black – system with ConAC dynamics, red – system without ConAC dynamics; a) Step responses; b) Pole maps.

Finally, full modal analysis is done on the newly-created, reduced-order system. It has been noted that *Mode 29* frequency and damping are not sensibly affected by ignoring ConAC line dynamics. Also, ranking of the most important states influencing *Mode 29*, and their associated participation factors are the same as in the full-order case.

The above observations gathered from the step responses, pole maps and modal analysis allow us to state that the dynamics of ConAC line, interconnecting the two HVDC lines do not significantly affect the interconnection *Mode*

29. Therefore, simulations of large power systems that include HVDCs would not require complete dynamic modeling of AC lines. Static models that employ equations (13) are sufficient in order to properly capture the behavior of interconnected HVDC lines. This will significantly reduce the computation burden associated with the simulation of large power systems that embody a large number of lines.

6.2 System with instantaneous inner (current) VSC loop dynamics

Here, the low-level inner control loops for i_d and i_q currents are reduced to instantaneous current sources. As previously, the effect of this model reduction will be assessed *vs* the initial full-order model.

To this end, in the benchmark containing HVDC interacting links one uses directly the variables i_{dk}^* and i_{qk}^* , with $k = 1, \dots, 4$ (current references for all HVDC stations) both in the AC lines equations and in the ones that give the active and reactive power values P_k and Q_k . PLL dynamics are taken into account here, as variables i_{dk}^* and i_{qk}^* need coordinate (Kron) transform.

In this case, dynamic interaction between S1 and S2 and between S3 and S4 are completely decoupled: currents i_{dq} at station S1 do not depend anymore on the v_{DC} voltage, which is a variable shared with S2; hence, this later (given by the model of S2) does not influence dynamics at station S1. This implies that HVDCs interaction is reduced only to interaction between models of stations S1 and S3.

If the model reduction applies only to station S1, *i.e.*, $i_{1d} \equiv i_{1d}^*$ and $i_{1q} \equiv i_{1q}^*$, a 38th order system is obtained by using the same procedure as in previous cases. Fig. 10 a) gives the step response of the reduced-order linearized system (in blue line) plotted *vs* the one of the original system (plotted with red line). Note that the reduced-order system is much more damped. The same effect is seen on Fig. 10 b) which provides the pole maps of reduced-order system (blue crosses) *vs* the one of the original system (with red crosses). Note that many of the poles, including the pole of interest, are missing from the reduced-order system.

Table 5 shows two modes of the reduced-order linearized system in the frequency range of interest. The mode closest in frequency to the *Mode 29* of the full-order system is one of 19,89 Hz, in which participate mostly states from inner loops associated to stations S3 and S4. Thus, this is not a coupling mode via the grid.

The above-presented analysis clearly shows that the system simplification by neglecting low-level current loops yields a reduced-order system which does not retain any longer specific behavior of the two interacting HVDC lines, analyzed in previous sections of this report. The mode of interest (*Mode 29*) is no more present in the reduced-order system, the overall response is more damped, the system is farther from instability *wrt.* the original, full-order case.

6.3 System with instantaneous PLL dynamics

In this section PLL dynamic behavior is neglected. The PCC angle is directly computed in numerical simulation by using equations set (1). For station S1, these equations output voltage components at PCC1 as $v_{d1} \equiv v_{rd1}$ and $v_{q1} \equiv v_{rq1}$ and one may compute the PCC1 voltage angle as:

$$\delta_1 = -\arctan\left(\frac{v_{q1}}{v_{d1}}\right).$$

This angle is then used in Kron transform to obtain voltage and current images in the PLL dq frame to be used in control algorithm.

The nonlinear system step response with such an ideal PLL for station S1 is given in Fig. 11 a), with blue line. Note that the response is significantly more damped *wrt.* the case of the full-order original system. Fig. 11 b) shows the

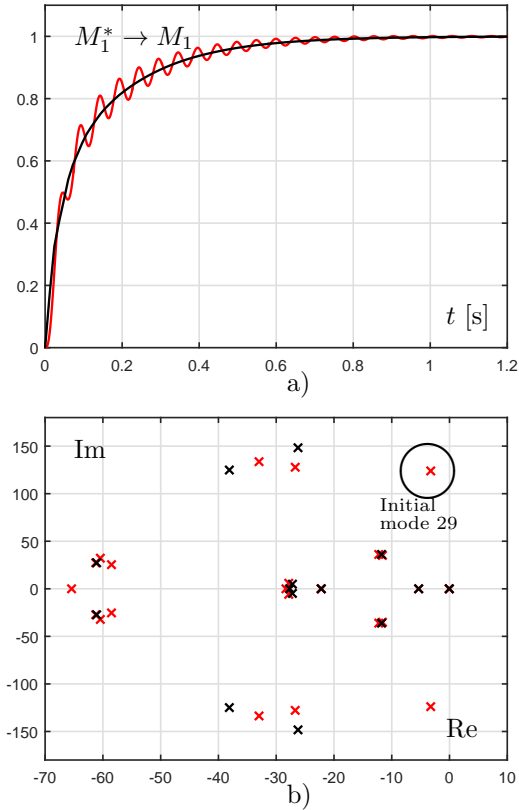


Figure 10: Red – system with i_{dq} dynamics, black – system without i_{dq} dynamics at station S1; a) Step responses; b) Pole maps.

displacement of the oscillatory pole in the complex plane – see the blue crosses *wrt.* the red crosses (the full-order model). The measured damping is 0.088.

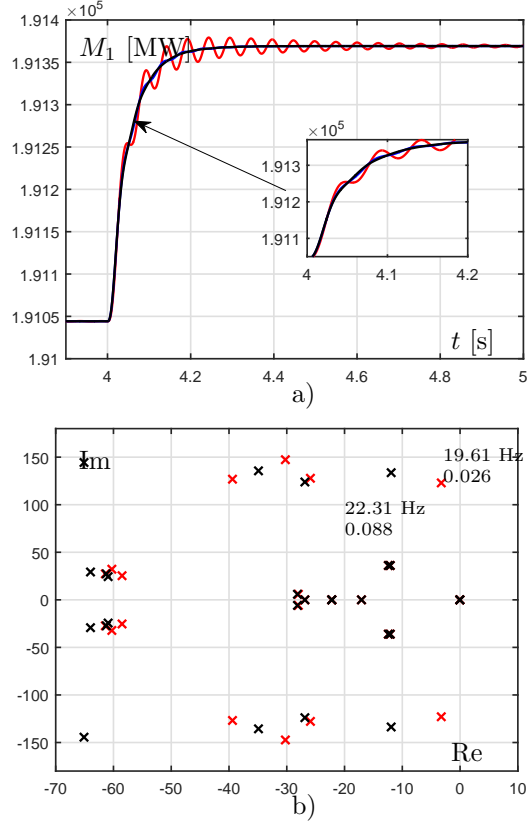


Figure 11: Red – system with PLL dynamics, black – system without PLL dynamics on S1 only; a) Step responses; b) Pole maps.

Table 6 comparatively shows ranking of states involved in the mode of interest. The case of the full-order system is in the left side and the case with instantaneous PLL at station S1 is in the left side. Note that frequency and damping of the mode differ significantly. Ranking of states and participation factors in *Mode 29* differ significantly to the point that this mode involves only variables of station S1, *i.e.*, it is no longer a coupling mode between the two HVDCs.

To conclude, the above presented analysis clearly shows that the system simplification by neglecting the PLL dynamics yield a reduced-order system that does not retain any longer the specific behavior of the two interacting HVDC lines, analyzed in previous sections of this report. The *Mode 29* of interest is significantly shifted in the reduced-order system (depending of the number of neglected PLLs), the overall response is more damped, the system is farther

from instability *wrt.* the original, full-order case.

7 Analysis in the case of AC grid with synchronous generator

Next, a controlled synchronous generator has been inserted in the dual HVDC benchmark, as shown in Fig. 1. In the new structure one actually splits AC1 impedance into two equivalent RL lines, in order to obtain sound comparison base with the previous case. The synchronous generator is inserted closer to station S1 than the infinite bus such that *AC line 6* is about 50 km and *AC line 5* is 150 km.

The target here is to apply the mixed approach described in Section 3 to the entire system in Fig. 1, including not only the two HVDC links, but also the synchronous generator. Basically, all the operations and analysis made on the previous case are repeated for this new set-up. ConAC length is 150 km. SCR1=3.5 and SCR3=3 (which makes a slight structural unbalance between S1 and S3). Setpoint voltages at Stations S1-S4 are at their rated values. Steady-state operating point corresponds to $P_1 = -500$ MW and $P_3 = +600$ MW. Steps of reference voltage, M_1^* , are applied at S1 for observing the overall system dynamic behavior.

7.1 Interaction mode identification

7.1.1 Case 1 – positive M_1^* step of 10% of rated value of M_1

Fig. 12 shows the overall system (*i.e.*, the one containing also synchronous generator G1) behavior, with red color *vs* the one formed only by the two interacting HVDC links, with black color. The focus is here on the variables belonging to HVDC stations. The new system is not significantly faster than the old one. Moreover, one observes that the system including generator G1 behavior is less damped *wrt.* the original one, the system has even smaller stability reserve. In this new case, the coupling oscillatory mode has frequency of ≈ 18 Hz with damping smaller than 10%. Supplementary simulations show that these parameters depend on the steady-state operating point (signs and values of P_1 , P_3 and P_e variable).

7.1.2 Case 2 – negative M_1^* step of 5% of rated value of M_1

Fig. 13 shows the system response, the focus being here on the generator behavior. Note that the oscillatory mode can be observed in the generator's power, P_e : it is the spike at moment 50 s. The other lower frequency mode is about 0.25 Hz.

These time-domain simulations have shown that overall system dynamics are changing when a synchronous generator is inserted in the AC grid (in this case within the line AC1). So, a new modal analysis will be done in this section,

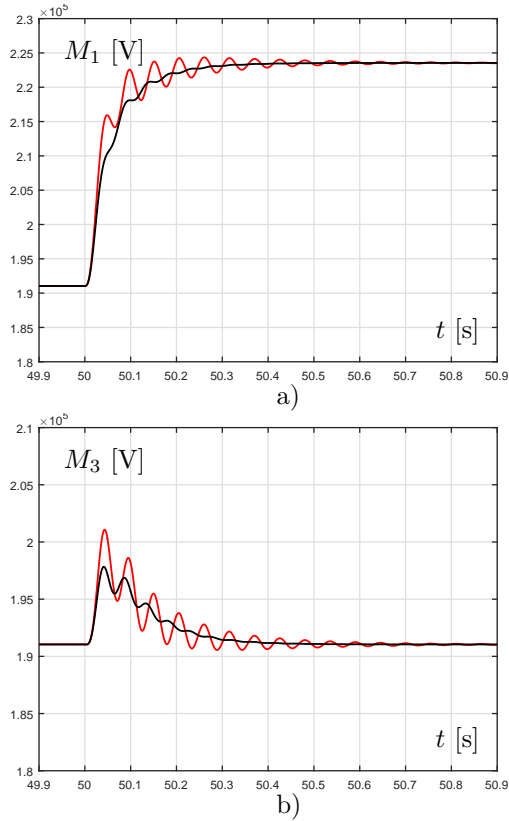


Figure 12: System response to a voltage reference step at S1: red – interacting HVDC links including generator G1; black – interacting HVDCs without generator G1. Evolutions of: a) S1 voltage, M_1 ; b) S3 voltage, M_3 .

in order to full assess the behavior of this system. The main target is the high-frequency mode (situated in the neighborhood of 20 Hz), which is similar to *Mode 29* of the original system and which will be further denoted as *Mode 38*.

7.2 Modal analysis

Linearization around a certain operating point has been done numerically for each subsequent scenarios and a new linear model with 72 states, whose parameters depend on the current scenario, is obtained.

Table 7 shows *Mode 38* parameters – in the case with generator, at the left side – *vs Mode 29* parameters, without generator – at the right side, for various active power flows. Note that generator currents have important participation factors, and mode parameters (frequency and damping) significantly differ. But new frequency is not much lower, 18.5 Hz *vs* 20.5 Hz, but the reduction in

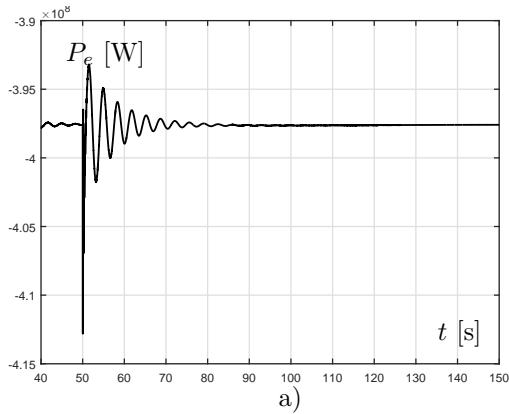


Figure 13: output generator power P_e response to a voltage reference step at S1

damping is very important (*i.e.*, from 8% to 0.6%). Basically, one observes here the same phenomenon like in the previous case of HVDCs interaction without synchronous generator – see Sections 4 and 5.

Also, insertion of the generator breaks the link between the participating stations and the sign of the power flow, observed in the previous case (without generator). In this sense, Table 7 shows that station S4 has been excluded from the participation top ranking; its states have been replaced by ones belonging to the generator.

Therefore, synchronous generator insertion in the benchmark containing the two HVDC links changes the interaction behavior, and modifies the parameters of the main oscillatory mode. The frequency becomes slightly lower (*e.g.*, from 20 Hz to 18 Hz) and the damping becomes smaller. Some operating regimes (at high level of active power values or in the case where both S1 and S3 inject active power) become unstable, which reduces system effective operating range.

Acknowledgment

The authors would like to thank Dr. Hani Saad from Réseau de Transport d'Electricité (RTE) de France for his useful remarks on the manuscript.

8 Conclusion

This paper has dealt with analysis of two close-connected HVDC lines by using high-fidelity models in dq frame.

A potentially inconvenient interaction, due to HVDCs coupling, has been highlighted through time-domain simulation. Modal analysis has shown that this interaction consists in an oscillatory (*i.e.*, complex) mode between converters of distant HVDCs. The low-level controllers and PLLs states have the high-

est participations in this coupling oscillatory mode. A quite exhaustive study of the variation of the parameters of the system, as well as the modification of the control structure, have shown that this mode exists in all situations, *i.e.*, it is related to a *structural* coupling phenomena. Only its damping varies with the parameters of the system (it is smaller as AC grid SCRs decrease) and, in general, depends on the power flow. It may be under 5% if both AC-linked stations inject active power into the grid, or if synchronous generators are present in the system. It has also been shown that this coupling phenomena can be accurately captured with transient-stability models, *i.e.*, neither dynamic models for the AC lines, nor high-frequency (to capture the switchings) representation of the converters are necessary. This significantly facilitates the analysis in a realistic (large-scale) grid context, as needed by TSOs to state the stability and coordination of controls. Of course, high-order harmonics aspect should be studied apart, with higher-frequency models.

To some extent, this kind of interaction mode is similar to the well-known inter-area modes existing between rotating generators.

Even if the study is done on a system with simple topology, the main characteristics of real situations are captured by the AC lines which connect the two HVDCs and the infinite buses. This models the electrical distance on a real power system and it is expected that the conclusions above hold in the general case.

The way in which the control should be adapted to damp this kind of modes in critical situations is now under development and will be presented in forthcoming publications.

9 Symbols used

int PI iq1 – i_q PI controller at S1 – see 2nd eq. of (6)
int PLL1 – integrator of phase locked loop at S1 – see Fig. 3
int PI id3 – i_d PI controller at S3 – see 1st eq. of (6)
Reactor1/int iq – i_q current of reactor at S1 – see 2nd eq. of (1)
Reactor 3/int iq – i_q current of reactor at S3 – see 2nd eq. of (1)
int PI id4 – i_d PI controller at S3 – see 1st eq. of (6)
int PLL4 – integrator of phase locked loop at S4 – see Fig. 3
int PI PLL1 – integrator of PI controller of PLL at S1 – see Fig. 3
AC line 1/int iq – i_q of line AC1 (linked to S1) – see 5th eq. of (1)
AC line 4/int id – i_d of line AC4 (linked to S4) – see 4th eq. of (1)
Prefilter id2 – prefilter for i_d PI controller at S2 – see 1st eq. of (6)
int PI vdc4 – integrator of v_{DC} PI controller at S2 – see eq. (7)
DC filter 3/int 1 – state of HVDC capacitor – see 3rd eq. of (1)
int id – integrator of AC generator’s stator current equation, i_d
int if – integrator of AC generator’s field current equation i_f
int M1 – M integral controller at S1 – see 4th eq. of (6)

References

- [1] Flourentzou, N., Agelidis, V. G., and Demetriades G. D.: 'VSC-based HVDC power transmission systems: An overview', *IEEE Transactions on power electronics*, 2009, 24, (3), pp. 592-602
- [2] 'INELFE Consortium – France-Spain HVDC link', <http://www.inelfe.eu/en/projects/baixas-santa-llogaia/>, accessed March 2018
- [3] Bui, L. X., Sood, V. K., and Laurin, S.: 'Dynamic interactions between HVDC systems connected to AC buses in close proximity', *IEEE Transactions on Power Delivery*, 1991, 6, (1), pp. 223-230
- [4] Henry, S., Despouys, O., Adapa, R., Barthold, L., Bayfield, C., Bell, K., ... and Irwin, G: CIGRE JWG C4/B4/C1.604., 'Influence of embedded HVDC transmission on system security and AC network performance' (CIGRE, 2013), pp. 1-267
- [5] Davies, B. *et al.*: CIGRE JWG B4.41. 'Systems with multiple DC infeed' (CIGRE, 2007), pp. 1-117
- [6] Bayo-Salas, A., Beerten, J., Rimez, J., and Van Hertem, D.: 'Impedance-based stability assessment of parallel VSC HVDC grid connections'. Proc. 11th IET International Conference on AC and DC Power Transmission, February 2015, pp. 1-9
- [7] Pinares, G., and Bongiorno, M.: 'Modeling and analysis of VSC-based HVDC systems for dc network stability studies', *IEEE Transactions on Power Delivery*, 2016, 31, (2), pp. 848-856
- [8] Beerten, J., D'Arco, S., and Suul, J. A.: 'Identification and small-signal analysis of interaction modes in VSC MTDC systems', *IEEE Transactions on Power Delivery*, 2016, 31, (2), pp. 888-897
- [9] Arioua, L., and Marinescu, B.: 'Multivariable control with grid objectives of an HVDC link embedded in a large-scale AC grid', *International Journal of Electrical Power & Energy Systems*, 2015, 72, pp. 99-108
- [10] Munteanu I., Marinescu B. and Xavier F.: 'Analysis of the interactions between close HVDC links inserted in an AC grid'. Proc. of the 2017 IEEE Power & Energy Society General Meeting, Chicago, Illinois, USA, July 2017, pp. 1-5
- [11] Rogers G.: 'Power system oscillations' (Springer Science & Business Media, 2000)
- [12] Saad, H., Mahseredjian, J., Dennetière, S., and Nguéfeu, S.: 'Interactions studies of HVDC-MMC link embedded in an AC grid', *Electric Power Systems Research*, 2016, 138, pp. 202-209

- [13] CIGRE WG 33.02., 'Guidelines for representation of network elements when calculating transients' (CIGRE, 1990), pp. 1-30
- [14] R. D. Middlebrook and S. Cuk: 'A general unified approach to modeling switching power converter stages', Proc. IEEE PESC, June 1976, pp. 18-34
- [15] Blasko, V., and Kaura, V.: 'A new mathematical model and control of a three-phase AC-DC voltage source converter', IEEE transactions on Power Electronics, 1997, 12, (1), pp. 116-123
- [16] Wang, W., Beddard, A., Barnes, M., and Marjanovic, O.: 'Analysis of active power control for VSC-HVDC', IEEE Transactions on Power Delivery, 2014, 29, (4), pp. 1978-1988
- [17] Padiyar, K. R.: 'Analysis of subsynchronous resonance in power systems' (Springer Science & Business Media, 1999)
- [18] RTE France: 'Voltage regulation and constructive capacities in reactive power of generation installations', Reference technical documentation (in French: Documentation technique de référence), 2016, pp. 1-1519
- [19] Wen, B., Boroyevich, D., Mattavelli, P., Shen, Z., and Burgos, R.: 'Influence of phase-locked loop on input admittance of three-phase voltage-source converters'. Proc. 28th Annual IEEE Applied Power Electronics Conference and Exposition (APEC), March, 2013, pp. 897-904.
- [20] Bacha, S., Munteanu, I., and Bratcu, A. I.: 'Power electronic converters modeling and control' (Advanced Textbooks in Control and Signal Processing, Springer, 2014)
- [21] Franken, B. and Andersson, G.: 'Analysis of HVDC converters connected to weak AC systems', IEEE Transactions on Power Systems, 1990, 5, (1), pp. 235-242
- [22] Kundur P.: 'Power Stability and Control' (McGraw-Hill, New York, 1994)
- [23] IEEE Std 421.5-2005: 'IEEE Recommended Practice for Excitation System Models for Power System Stability Studies', (Revision of IEEE Std 421.5-1992), 2006
- [24] Garofalo, F., Iannelli, L., and Vasca, F. : 'Participation factors and their connections to residues and relative gain array', IFAC Proceedings Volumes, 2002, 35, (1), pp. 125-130
- [25] D'Arco, S., Suul, J. A., and Fosso, O. B.: 'Small-signal modeling and parametric sensitivity of a virtual synchronous machine in islanded operation' International Journal of Electrical Power & Energy Systems, 2015, 72, pp. 3-15

Table 1: *Mode 29* parameters variations: left side – with SCR values, right side – with P_1 and P_3 values.

SCR	Freq. [Hz]	Damp.	P_1, P_3 [MW]	Freq. [Hz]	Damp.
3	19.6	0.034	-500, -600	19.57	0.021
4	21.6	0.096	-500, +600	21.5	0.08
5	22.94	0.131	+500, -600	21.27	0.084
-	-	-	+500, +600	22.08	0.081

A Appendix: System parameters

- AC system: frequency 50 Hz, rated RMS voltage 400 kV,
- AC line: resistance 0.03 Ω /km, inductance 0.79 mH/km,
- Transformer: secondary RMS voltage 230 kV, ratio 1.74, $R_{pr} = 0.4 \Omega$, $L_{pr} = 38$ mH, $R_{sec} = 0.132 \Omega$, $L_{sec} = 12.6$ mH,
- Line reactor: impedance 25.3 mH, resistance 0.08 Ω ,
- DC line: voltage 640 kV, capacitor 220 μF , resistance 13.9 m Ω /km, impedance 0.159 mH/km, length 200 km,
- VSCs: active power 1000 MW, reactive power $Q \in \{-500; +400\}$ MVar, maximum active current ± 4 kA, maximum reactive current ± 1.6 kA,
- Control parameters: $\lambda = 13e-6$ V/VAr, $T_{ic} = 6.6$ ms, $K_{pc} = 0.6e-4$ A $^{-1}$, $K_{tc} = 5 \cdot K_{tp} = 500$, $K_{pv} = 0.034$ A/V, $T_{iv} = 25$ ms, $T_{im} = 0.28$ s, $T_{ip} = 7.04$ ms,
- Synchronous generator:
 - $S_{rated} = 555$ MVA, $V_{Trated} = 24$ kV, $n_{tr} = 9.58$ (AC system RMS 230 kV),
 - $i_{frated} = 3500$ kA, $p = 1$, $J = 0.74e6$ kg \cdot m 2 , $F_r = 50$ N \cdot m \cdot s, $r_a = 3.1$ m Ω ,
 - $L_d = 4.98$ mH, $L_q = 4.845$ mH, $L_{afd} = 40$ mH, $r_f = 71.5$ m Ω $L_{ffd} = 576.9$ mH,
 - $R_{loc} = 11$ k Ω ,
- Synchronous generator control:
 - $T_{p1} = 10$ s, $G_p = 0.05$, $T_{p2} = 250$ s, $T_{mLim} = 1.6e6$ Nm, $T_{v1} = 100$ s, $T_{v2} = 10.5$ s, $G_V = 2.5$, $T_{v3} = 500$, $T_{v4} = 5$ s, $T_{v5} = 0.25$ s, $V_{fLim} = 1000$ kV.

Table 2: States influences in *Mode 29* for two values of SCR.

SCR → 5		SCR → 3	
State name	Participation	State name	Participation
int PI iq1	0.09	int PLL1	0.15
int PLL1	0.09	int PI iq1	0.14
int PI iq3	0.09	int PLL3	0.13
int PLL3	0.08	int PI iq3	0.13
int PI id1	0.06	int PI id3	0.09
Reactor 1/int iq	0.07	int PI id1	0.1
Reactor 3/int iq	0.05	Reactor 1/int iq	0.09
int PI id4	0.05	Reactor 3/int iq	0.07
int PLL4	0.05	int PI PLL1	0.06
int PI iq4	0.05	AC line 1/int iq	0.05

Table 3: States with largest participation in *Mode 29* for various P_1 and P_3 steady-state values.

P_1, P_3 [MW] -500, -600		P_1, P_3 [MW] 500, 600		P_1, P_3 [MW] 500, -600		P_1, P_3 [MW] -500, 600	
State name	Part.	State name	Part.	State name	Part.	State name	Part.
int PLL1	0.13	int PI iq4	0.07	int PI id2	0.17	int PI id4	0.14
int PLL3	0.13	int PI id4	0.07	int PLL2	0.15	int PLL4	0.12
int PI iq3	0.13	int PLL4	0.07	int PI iq2	0.14	int PI iq4	0.12
int PI iq1	0.12	int PI id2	0.06	int PLL3	0.1	Reactor4/int iq	0.09
int PI id3	0.1	int PLL2	0.06	int PI iq3	0.1	int PLL1	0.07
int PI id1	0.09	int PI iq2	0.05	Reactor2/int iq	0.1	int PI iq1	0.07
Reactor3/int iq	0.08	Reactor4/int iq	0.05	Reactor2/int id	0.09	Reactor4/int id	0.07
Reactor1/int iq	0.08	Reactor2/int iq	0.04	AC line2/int id	0.07	Prefilter id4	0.06
AC line3 /int iq	0.05	int PLL1	0.04	Prefilter id2	0.07	AC line4 /int id	0.06
int PI PLL3	0.05	int PI iq1	0.04	Reactor3/int iq	0.07	Reactor1/int iq	0.05
AC line1/int iq	0.05	int PLL3	0.04	int PI id3	0.07	int PI id1	0.05
int PI PLL1	0.05	int PI iq3	0.04	int PI iq1	0.06	int PI PLL4	0.04

Table 4: Total sensitivity of *Mode 29* wrt. ConAC length for various active power levels.

P_1, P_3 [MW]	-500, -500	-500, +500	+500, -500	+500, +500
$S_{L29} = \sum s_{kl}$	3.4e-6	6.74e3	5.92e3	2.15e-6

Table 5: Ranking of states for two oscillatory modes closed to the domain of interest of linearized reduced-order system in the case where only station S1 has no current dynamics.

Freq. 19,89 [Hz] – Damp. 0,292		Freq. 5,68 [Hz] – Damp. 0,314	
int PI id4	0,21	int PI vdc4	0,5
int PI iq4	0,18	Prefilter id4	0,17
int PLL4	0,16	int PI id3	0,16
Reactor4/int id	0,12	int P3	0,13
int PI id3	0,11	DC filter3/int2	0,1
int PI iq3	0,09	DC filter3/int1	0,1
AC line4/int id	0,08	DC filter4/int2	0,09
int PLL3	0,08	DC filter4/int1	0,09
int PI PLL4	0,06	int PI id4	0,09

Table 6: Ranking of states for the interaction mode. Left side – the case of the original full-order system; right side – the case with neglected dynamics of PLL1.

PLL1– PLL4 with dynamics		PLL1 without dynamics	
Freq. 19,61 [Hz] – Damp. 0,026 (<i>Mode 29</i>)		Freq. 21,31 [Hz] – Damp. 0,088	
int PLL3	0,13	int PI iq3	0,2
int PI iq3	0,13	int PLL3	0,2
int PLL1	0,13	Reactor 3/int iq	0,14
int PI iq1	0,12	int PI id3	0,12
int PI id3	0,1	int PI PLL3	0,07
int PI id1	0,09	Reactor 4/int id	0,07
Reactor 3/int iq	0,09	Prefilter id4	0,06
Reactor 1/int iq	0,08	AC line 3/int iq	0,06
AC line 3/int iq	0,05	int PI id4	0,06

Table 7: *Mode 29* parameters (left side) vs *Mode 38* parameters (right side) – case where $P_1 = -500$, $P_3 = +600$ MW.

Freq. 21,6 [Hz] – Damp. 0,08		Freq. 18,41 [Hz] – Damp. 0,006	
int PI id4	0,12	int id	0,42
int PLL4	0,11	int if	0,42
int PI iq4	0,11	int PLL1	0,19
int PLL1	0,08	int PI iq1	0,19
Reactor 4/int iq	0,08	int PI id1	0,12
int PI iq1	0,08	Reactor 1/int iq	0,09
Reactor 4/int id	0,06	int PI iq3	0,08
Prefilter id4	0,05	int PLL3	0,08
Reactor 1/int iq	0,05	int PI PLL1	0,08
AC line 4/int id	0,05	int M1	0,07